

A model-based method for the characterisation of stress in magnetic materials using eddy current non-destructive evaluation

Abla Dahia, Eric Berthelot, Yann Le Bihan and Laurent Daniel

Group of Electrical Engineering-Paris (GeePs), UMR 8507 CNRS, CentraleSupélec, Université Paris-Sud—UPMC, 11 rue Joliot-Curie, Plateau de Moulon, 91192 Gif-sur-Yvette, France

E-mail: abla.dahia@centralesupelec.fr

Received 17 November 2014, revised 5 February 2015

Accepted for publication 2 March 2015

Published 2 April 2015



Abstract

A precise knowledge of the distribution of internal stresses in materials is key to the prediction of magnetic and mechanical performance and lifetime of many industrial devices. This is the reason why many efforts have been made to develop and enhance the techniques for the non-destructive evaluation of stress. In the case of magnetic materials, the use of eddy current (EC) techniques is a promising pathway to stress evaluation. The principle is based on the significant changes in magnetic permeability of magnetic materials subjected to mechanical stress. These modifications of magnetic permeability affect in turn the signal obtained from an EC probe inspecting the material. From this principle, a numerical tool is proposed in this paper to predict the EC signal obtained from a material subjected to stress. This numerical tool is a combination of a 3D finite element approach with a magneto-mechanical constitutive law describing the effect of stress on the magnetic permeability. The model provides the variations of impedance of an EC probe as a function of stress. An experimental setup in which a magnetic material subjected to a tension stress is inspected using EC techniques is tailored in order to validate the model. A very good agreement is found between experimental and modelling results. For the Iron-Cobalt alloy tested in this study, it is shown that a uniaxial tensile stress can be detected with an error lower than 3 MPa in the range from 0 to 100 MPa.

Keywords: eddy current probe, non-destructive testing, residual stress, magnetostriction, magneto-elasticity

(Some figures may appear in colour only in the online journal)

1. Introduction

Internal stresses are a determinant factor to magnetic and mechanical performance, structural integrity and lifetime of industrial systems. Many techniques have therefore been developed for stress evaluation [1]. Among non-destructive evaluation (NDE) techniques, x-ray diffraction has become a standard [2, 3]. It remains however relatively expensive to carry out and requires specific operating conditions due to possible radiation hazard for personnel. In the case of magnetic materials, magnetic NDE techniques [4, 5] can offer an attractive alternative to x-ray diffraction. These techniques rely on the strong influence of stress on the magnetic

properties of magnetic materials [6, 7]. Several techniques for *in-situ* measurement on industrial parts have been developed [8–12]. They are usually based on the detection of a combination of stress-induced effects on magnetic properties such as magnetic permeability, coercivity or Barkhausen noise. They involve a preliminary characterisation of the tested materials to determine the phenomenological parameters of the empirical models used in the stress evaluation. Other techniques rely on the effect of stress on the residual magnetic field measured in the vicinity of magnetic materials [13–15]. Some authors focused on the detection of stress using EC techniques [16–18]. The approach relies on the high sensitivity of eddy currents (EC) signals to the magnetic permeability of

materials, itself highly dependent on stress. The EC technique has many advantages: it is simple to implement, easily automatable and cheap. However, efficient modelling tools are needed in order to design the EC probes and to analyse the EC signals recorded from inspections.

The purpose of this work is to develop a numerical tool to model the EC signal provided by an EC probe inspecting a material subjected to stress. The modelling is done in two steps. First, the effect of stress on the permeability is predicted using a simplified version of a multiscale model for magneto-elastic behaviour [19, 20]. Then, the EC probe signal is determined as a function of the permeability using the finite element method (FEM). The modelling results are compared to an EC NDE experimentation performed on an Iron–Cobalt alloy.

In the first part of this paper, the principle of the EC NDE is explained. In the second part, the modelling approach used to describe the effect of stress on the magnetic permeability is presented. The experimental EC characterisation device is then introduced and the corresponding FEM approach described. Experimental and numerical results are finally compared and discussed.

2. Non-destructive evaluation by eddy currents

Among other applications, the EC technique has been considered as a NDE method to evaluate stress in conductive materials, magnetic or not [17, 18, 21, 22]. The principle is to create an alternating magnetic field by means of an EC probe-coil positioned close to the material surface [23]. This magnetic field generates electrical currents (eddy currents) in the material. The EC depend on several factors such as material geometry, electromagnetic properties (electrical conductivity and magnetic permeability) and frequency of the excitation current. Any change in the material properties causes a perturbation in the EC flow. This disruption can be detected for example by measuring the EC probe impedance. The EC concentrate on the surface of the material under the EC probe. Their density decreases exponentially with respect to the depth from the surface into the material (figure 1) [24]. This phenomenon is known as the skin effect. The magnitude of the EC density at a depth z is given by:

$$J(z) = J_s e^{-z\sqrt{\pi f \mu \sigma}} = J_s e^{-\frac{z}{\delta}} \quad (1)$$

where

$$\delta = \frac{1}{\sqrt{(\pi f \mu \sigma)}} \quad (2)$$

is the skin depth. f is the excitation frequency, μ the magnetic permeability (assuming isotropic magnetic behaviour), σ the electrical conductivity of the material (assuming isotropic electrical behaviour), z the considered depth into the material and J_s the magnitude of the EC density at the material surface ($z = 0$).

In the case of ferromagnetic materials, the skin effect is strong due to the high value of the magnetic permeability.

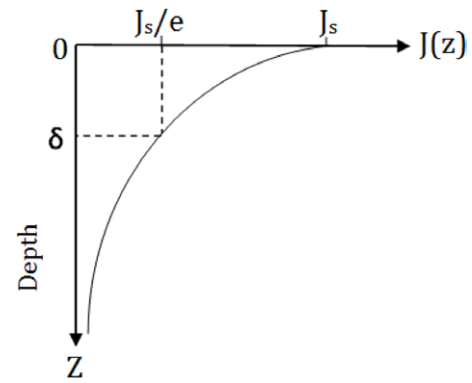


Figure 1. Variation of the magnitude of the EC density J with respect to the depth z from the surface into the material.

3. Magneto-mechanical behaviour

Magneto-mechanical couplings in magnetic materials are the result of complex mechanisms by which the application of stress modifies the domain structure and its evolution under external loading. They have many consequences on the macroscopic response of magnetic materials. The effect of stress is notably very significant on the magnetic permeability [6, 7]. This effect is sometimes called the Villari effect or inverse magnetostrictive effect. The proposed NDE method is based on this effect. In this paper, the evolution of the magnetic permeability under stress is first measured on an Iron–Cobalt alloy. A corresponding coupled constitutive law is then proposed.

3.1. Magnetic characterisation of the ferromagnetic sample

The material of interest in this work is a commercial Iron–Cobalt alloy for high-speed rotating machines. It is a soft ferromagnetic material composed of 49% Iron (Fe), 49% Cobalt (Co) and 2% Vanadium (V). The dimensions of the specimen are $112 \times 12.5 \times 2.5 \text{ mm}^3$. A magneto-mechanical test rig [25] is used to characterise the macroscopic behaviour (figures 2(a) and (b)). The magnetic field is generated by an excitation coil positioned around the sample and fed with an alternating current. A magnetic circuit consisting in two U-shaped Fe–Si cores having a large cross section ($18 \times 32 \text{ mm}^2$) is used to concentrate the magnetic flux. This allows creating a high magnetic field in the sample with a reasonable current in the excitation coil. The sample and the magnetic circuit are then installed between the collet grips of a tension/compression electro-mechanical machine Zwick/Roell Z030. This machine allows the application of uniaxial tensile/compression stress. In this study only tensile stresses have been considered and only the component of the relative permeability tensor along the applied stress direction (x -component) is determined by the measurement.

In order to perform the characterisation from a stable magnetic state, the specimen are demagnetised before each measurement. To achieve the demagnetisation, a sinusoidal current at low frequency (1 Hz) with a slowly exponentially decreasing magnitude is applied. The demagnetisation is performed using the same setup as for the characterisation (figures 2(a) and (b)). Once the material is demagnetised,

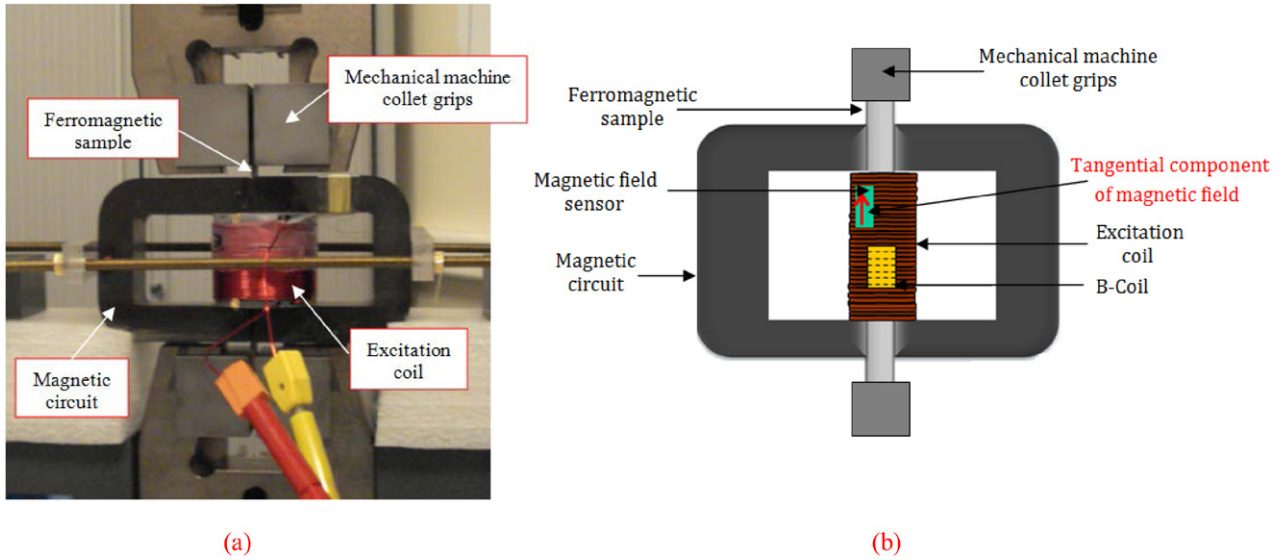


Figure 2. Picture (a) and drawing (b) of the test setup for the magneto-mechanical characterisation of ferromagnetic materials.

the tensile stress is applied, and the anhysteretic magnetisation curve is recorded. The procedure to obtain a point of the anhysteretic curve is similar as a demagnetisation procedure but with a constant bias magnetic field superimposed to the demagnetisation signal. The magnetic field \mathbf{H} inside the material is obtained from a fluxgate sensor positioned inside the excitation coil at the surface of the sample (the tangential component of \mathbf{H} being continuous at the interface between the material and air). The magnetic induction \mathbf{B} inside the material is obtained from a time integration of the induced voltage measured between the ends of a B-coil wound around the ferromagnetic sample inside the excitation coil. The x -component of the relative permeability of the sample is determined from the slope of the anhysteretic B-H curve. The same procedure is repeated for various levels of stress and the stress-dependent relative permeability is therefore determined. In all the study, the tensile stress level is maintained lower than the yield stress of the material (approximately 300 MPa) so as to remain in the elastic regime.

3.2. Material modelling

The stress-dependent magnetic permeability is modelled using a simplification of a multiscale model for anhysteretic magneto-elastic behaviour [19, 20]. The multiscale model is based on an energetic description of the magneto-elastic equilibrium at the magnetic domain scale. Scale transition rules allow linking the macroscopic scale—at which an average constitutive law is defined—to the local scale—at which the relevant physical mechanisms can be described. It gives a prediction of the reversible (anhysteretic) response of magnetic materials subjected to multiaxial magneto-mechanical loadings. In this work, in order to reduce computation time and facilitate an implementation into FEM tools, a simplified magneto-elastic model (SMM) is proposed. It is a 3D extension of a 2D version previously published [26] and is similar to Armstrong’s approach [27]. Compared to the full-multiscale model, additional assumptions are considered. The material is considered

Table 1. Material parameters used for the simplified magneto-elastic model.

M_s ($A\ m^{-1}$)	λ_s	A_s ($m^3\ J^{-1}$)
1.8×10^6	37×10^{-6}	2.8×10^{-3}

as a set of magnetic domains randomly oriented. The potential energy of the material (equation (3)) is defined as the sum of three contributions. The magneto-static energy (equation (4)) tends to align the magnetisation with the applied field, the magneto-elastic energy (equation (5)) describes the effect of stress on the behaviour. An anisotropy energy (equation (6)) can be added to describe macroscopic anisotropy effects for example resulting from the combination of crystalline anisotropy and crystallographic texture.

$$W_\alpha = W_\alpha^{\text{mag}} + W_\alpha^{\text{el}} + W_\alpha^{\text{an}} \quad (3)$$

$$W_\alpha^{\text{mag}} = -\mu_0 \mathbf{H} \cdot \mathbf{M}_\alpha \quad (4)$$

$$W_\alpha^{\text{el}} = -\mathbf{T} : \boldsymbol{\epsilon}_\alpha^\mu \quad (5)$$

where the symbol ‘:’ denotes the tensor product (double contraction).

$$W_\alpha^{\text{an}} = K(\mathbf{u}_\alpha \cdot \boldsymbol{\beta})^2 \quad (6)$$

μ_0 is the vacuum permeability, \mathbf{H} and \mathbf{T} are the applied magnetic field and stress, \mathbf{M}_α and $\boldsymbol{\epsilon}_\alpha^\mu$ are the local magnetisation and magnetostriction strain at the domain scale. The anisotropy energy is given for a uniaxial anisotropy along direction $\boldsymbol{\beta}$, \mathbf{u}_α being the magnetisation direction (unit vector) in a domain α , and K is a constant to be determined. The local magnetisation \mathbf{M}_α in a domain α is given by (equation (7)) with M_s the saturation magnetisation of the material. The magnetostriction strain second order tensor $\boldsymbol{\epsilon}_\alpha^\mu$ is given by (equation (8)), with λ_s the saturation magnetostriction constant and \mathbf{I} the second order identity tensor.

$$\mathbf{M}_\alpha = M_s \mathbf{u}_\alpha \quad (7)$$

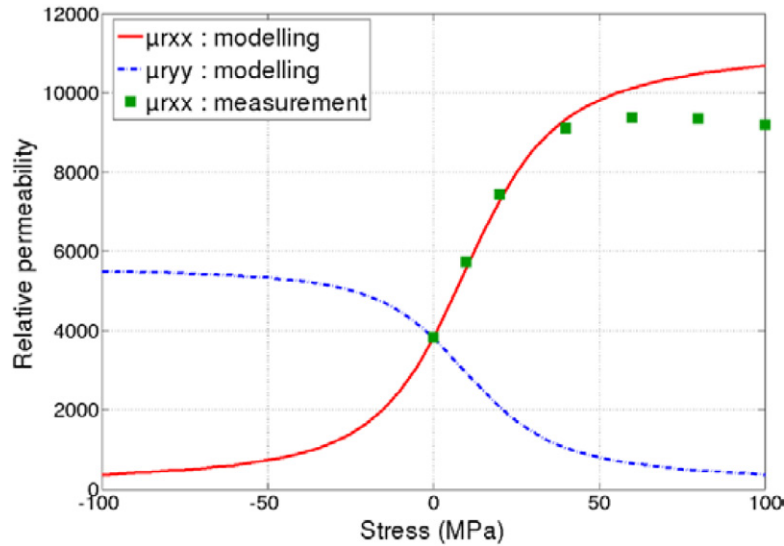


Figure 3. Effect of stress on the magnetic permeability: modelling of the x - and y -components (μ_{rxx} , μ_{ryy}) of the relative magnetic permeability tensor under uniaxial tensile/compressive stress (lines) and measured x -component of the magnetic permeability under tensile stress (markers).



Figure 4. EC probe.

$$\boldsymbol{\epsilon}_\alpha^\mu = \lambda_s \left(\frac{3}{2} \mathbf{u}_\alpha \otimes \mathbf{u}_\alpha - \frac{1}{2} \mathbf{I} \right) \quad (8)$$

The volume fraction f_α of a domain with magnetisation oriented along \mathbf{u}_α is given by (equation (9)) using a Boltzmann type relation [28]:

$$f_\alpha = \frac{\exp(-A_s W_\alpha)}{\frac{1}{V} \int_V \exp(-A_s W_\alpha) dV} \quad (9)$$

where V is the considered volume element, A_s is an adjustment parameter linked to the initial anhysteretic susceptibility χ^0 : $A_s = 3\chi^0/(\mu_0 M_s^2)$ [19]. The macroscopic magnetisation \mathbf{M} and magnetostriction $\boldsymbol{\epsilon}^\mu$ are then obtained by the volume average (equations (10) and (11)).

Table 2. EC probe characteristics.

Coil turn number	2×123
Coil height	1 mm
Coil cross-section	1×0.45 mm
Core height	3 mm
Core relative permeability	1100
Pole cross-section	1×1 mm
Pole air-gap	1 mm

$$\mathbf{M} = \langle \mathbf{M}_\alpha \rangle = \frac{1}{V} \int_V f_\alpha \mathbf{M}_\alpha dV \quad (10)$$

$$\boldsymbol{\epsilon}^\mu = \langle \boldsymbol{\epsilon}_\alpha^\mu \rangle = \frac{1}{V} \int_V f_\alpha \boldsymbol{\epsilon}_\alpha^\mu dV \quad (11)$$

From a practical point of view the integration is performed using a discrete mesh of a unit sphere to describe the possible orientations for the local magnetisation direction \mathbf{u}_α [20].

Therefore, in the case of an initially isotropic material, the model relies on three material parameters M_s , λ and A_s . It has been applied to the Iron–Cobalt alloy of this study. The material parameters are given in table 1.

The parameter A_s has been determined from the initial anhysteretic susceptibility of the measured anhysteretic curve under no applied stress. Figure 3 shows the results obtained with the SMM for the two in-plane components μ_{rxx} , μ_{ryy} (parallel and perpendicular to the applied stress direction, respectively) of the relative permeability tensor as a function of the uniaxial stress applied along the x -axis. The measured permeability under uniaxial tensile stress is also shown.

As already reported in the literature, it can be observed that the effect of stress is non-linear and non-symmetric in

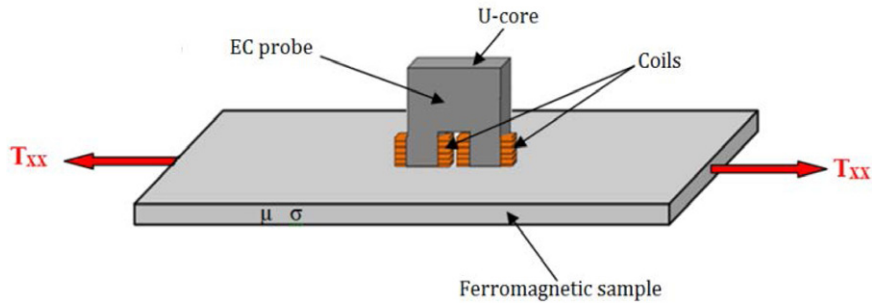


Figure 5. Studied problem.

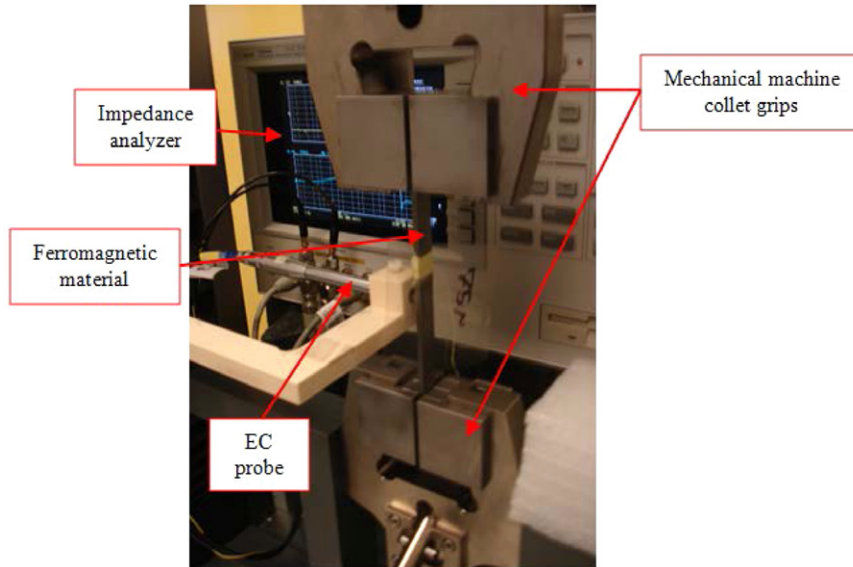


Figure 6. Test-rig for EC measurements under stress.

tension/compression. After an increase with the magnitude of tensile stress, the magnetic permeability seems to saturate and even to reverse. This effect was attributed in [29] to the effect of stress on the initial domain configuration. It is not included and therefore not reproduced by the SMM which tends to overestimate the permeability along the tension axis. The stress-induced anisotropy, not measured in the study, is also predicted by the SMM. The SMM will be used in the following to predict the stress-induced anisotropic permeability of the material.

4. Eddy current characterisation device

The EC probe used in this study is constituted of two coils wound around the poles of an U-shaped ferrite core. The coils are connected in series with currents flowing in opposition of phase. The EC probe (figure 4 and table 2 for characteristics) is positioned close to the ferromagnetic sample on which the uniaxial stress T_{xx} is applied (see figure 5). The surface resolution of the stress distribution measurement is mostly defined by the sensor dimensions and is estimated in this work to be about $2\text{ mm} \times 2\text{ mm}$. The depth resolution is dependent on the material and on the frequency and is given by the skin depth (equation (2)).

A test-rig (figure 6) was designed in order to evaluate the effect of stress on the EC signal provided by the EC probe. The ferromagnetic sample is installed between the collet grips of the tension/compression machine. The EC probe is positioned close to the sample with a lift-off (distance between the EC probe and the sample) evaluated to $125\text{ }\mu\text{m}$. The probe is connected to an impedance analyser Agilent 4294A allowing the measurement of its impedance Z as a function of the stress level. The changes in impedance measurement under applied stress are attributed to the effect of stress on the magnetic permeability. The effect of stress on the electrical conductivity is assumed to be negligible, with changes of conductivity lower than 1% [30].

5. Experimental result

The measured relative variations of impedance with respect to the unstressed case $|Z(T_{xx}) - Z(0)|/|X(0)|$, where X is the imaginary part of the probe impedance, for different levels of tensile stresses ($T_{xx} = 50, 80$ and 100 MPa) is shown in figure 7. The variations of impedance are plotted as a function of the measurement frequency.

In order to explain the impedance variations obtained in figure 7, a simple magnetic reluctance equivalent circuit is used. In this circuit, NI is the magnetomotive force created

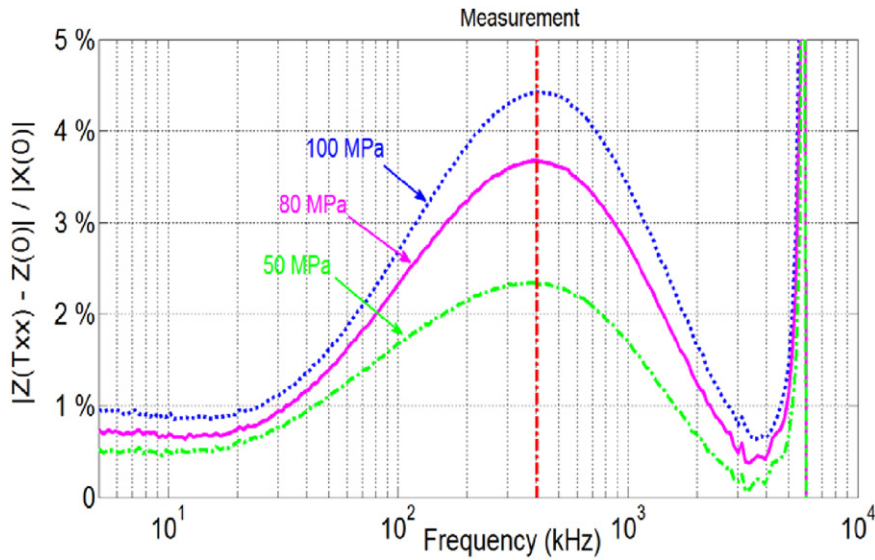


Figure 7. Measured variations of impedance Z for different levels of tensile stress (50, 80 and 100 MPa) as a function of frequency. The results are normalised by the reactance $X(0)$ in the unstressed configuration.

by the coil excitation (N turns fed by a current I), R_a is the air reluctance due to the lift-off (air-gap between the U-core and the magnetic material), R_m is the magnetic material reluctance, R_l is the leakage reluctance and Φ is the magnetic flux emitted by the probe. The reluctance of the U-core (connected in series with NI and R_a) is not taken into account since it is very low. The magnetic reluctance formula of a uniform flux tube is given by (equation (12)):

$$R = \frac{l}{\mu S} \quad (12)$$

where l is the length of the tube, μ the magnetic permeability and S the cross-sectional area of the tube. The equivalent reluctance seen in figure 8 by the probe is: $R_{eq} = R_a + (R_l // R_m)$. The probe impedance can then be deduced from R_{eq} as: $Z = R_0 + jN^2\omega / R_{eq}$ with R_0 the coil self-resistance (resistance due to the coil wire).

In figure 7, it can be noticed that at low frequencies (less than 20 kHz), the impedance variation is small, less than 1%. At such frequencies, the coil magnetic flux mainly penetrates into the magnetic material ($R_m \ll R_l$), because of the high permeability of the material and even if the skin depth in the material can be small (30 μ m at 20 kHz in absence of stress). Moreover, R_m is much lower than R_a . It results that $R_{eq} \approx R_a$ and the variation of R_m due to the level of stress has little effect on Z . From 20 kHz to approximately 400 kHz, the increasing skin effect in the magnetic material induces an increase of R_m because of a concomitant reduction of the flux tube section in the material (reduction of S in equation (12)). R_m then reaches the same order of magnitude as R_a , though being still lower than R_l . R_{eq} can then be written as $R_{eq} \approx R_a + R_m$ so that Z gets sensitive to the changes in the value of R_m due to the stress. Above 400 kHz up to 3 MHz, the still increasing skin effect leads to a supplementary increase of R_m which becomes higher than R_l . It follows that the majority of the magnetic flux does not penetrate the material and that $R_{eq} \approx R_a + R_l$. The effect of stress on Z becomes weak. The

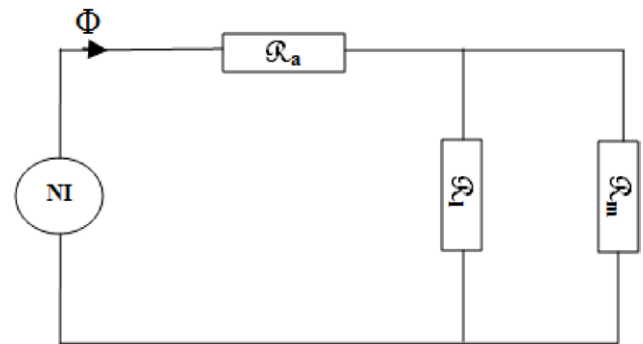


Figure 8. Reluctance equivalent circuit of the studied problem.

abrupt peak in the EC signal of figure 8 appearing at about 5 MHz corresponds to the probe coil resonance frequency due to the capacitive effects (turn-to-turn capacitances, turn-to-material capacitances) and cannot be exploited for stress evaluation since these capacitances are not related to the stress. The optimal operating frequency to reach maximum sensitivity for the stress detection is obtained when the impedance variations under stress are maximum. This optimum frequency is about 400 kHz in the present case. This frequency is very dependent on the considered problem and in particular on the inspected material. In this respect, a modelling tool predicting the EC signal of a probe inspecting a material subjected to stress is required to design an EC NDE procedure. The material used in this study (FeCoV) has a very high magnetic permeability so that the skin depth at the optimum frequency is small. It is expected that for many magnetic materials used in mechanical engineering with significantly lower magnetic permeability, the inspection depth of the proposed method will be higher.

6. Eddy current modelling

The FEM was chosen to model the effect of stress on the EC signal. This method is one of the most commonly used to approximate Maxwell's equations [31]. Compared to

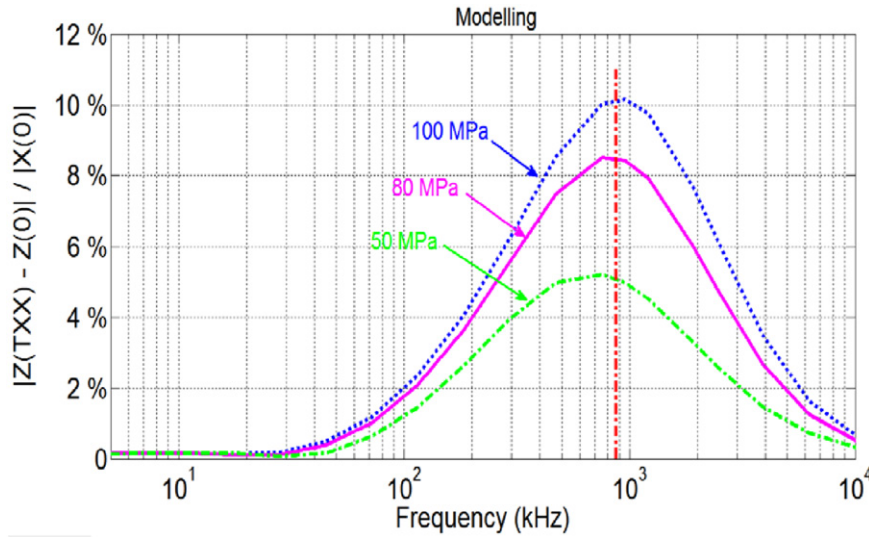


Figure 9. Simulated variations of impedance Z for different levels of tensile stress (50, 80 and 100 MPa) as a function of frequency. The results are normalised by the reactance $X(0)$ in the unstressed configuration. The material conductivity is taken as 3.84 MS m^{-1} .

analytical methods, it allows studying problems with complex geometry and anisotropic or non linear physical properties. Here, the FEM is used with a magnetic vector potential and an electrical scalar potential as degrees of freedom [32]. Considering the small excitation field used in EC NDE (about 10 A m^{-1}), a linear magnetodynamic calculation is implemented. Regarding the mesh, two kinds of elements are used: hexahedral elements to take readily into account the skin effect in the ferromagnetic material and tetrahedral elements for the other considered physical regions. Transition pyramid elements are created to connect hexahedral and tetrahedral sub-meshes. Due to the physical symmetries, only a quarter of the 3D problem is studied. In the considered application the mesh is constituted of approximately 2×10^5 elements. The problem was implemented into the commercial code ANSYS[®] using the anisotropic magnetic permeability obtained from the SMM as material properties. The observed probe signal is the impedance Z of the EC probe. This impedance is determined for its real part R from the power losses in the conducting domain (the ferromagnetic sample) and for its imaginary part X from the stored magnetic energy in the whole meshed domain ($Z = R + jX$).

7. Numerical result and discussion

The simulated relative variations of impedance with respect to the unstressed case $|Z(T_{xx}) - Z(0)|/|X(0)|$ for different levels of tensile stresses ($T_{xx} = 50, 80$ and 100 MPa) are shown in figure 9. The variations of impedance are plotted as a function of the measurement frequency. The electrical conductivity value is taken to be 3.84 MS m^{-1} according to independent results [33].

Simulated and measured results show very similar trends. The second peak due to probe-coil resonance is not reproduced in the modelling results. Indeed, the parasitic capacitances that appear at high frequencies are not taken into account in the magnetodynamic modelling. The peak frequency for

which the optimal sensitivity is found is not identical between measurement and simulation. A value of 870 kHz is found in the modelling to be compared to 400 kHz in the experiment. This difference can be attributed to an imprecise knowledge of the material electrical conductivity. Indeed a change of value of the electrical conductivity mainly induces a translation in the frequency response of the EC signal [24]. According to the classical approach [34], the total magnetic losses P_{tot} in a ferromagnetic material are the sum of three terms: hysteresis losses (static losses) P_{hyst} , EC losses P_{eddy} and excess losses P_{ex} (dynamic losses):

$$P_{\text{tot}} = P_{\text{hyst}} + P_{\text{eddy}} + P_{\text{ex}} \quad (13)$$

In the case of a sinusoidal excitation at frequency f with a maximum induction B , the total magnetic losses are expressed as:

$$P_{\text{tot}} = (K_h B^n f) + (K_c B^2 f^2) + (K_e B^{3/2} f^{3/2}) \quad (14)$$

where K_h , K_c , K_e and n are parameters depending on the material.

The excess losses are difficult to integrate in a magnetodynamic calculation; they can be partially taken into account by considering in the FEM modelling an equivalent conductivity higher than the DC conductivity of the material. This will increase the EC losses and better fit the real behaviour of the material.

This empirical approach was implemented. Figure 10 shows that considering an equivalent electrical conductivity of 7 MS m^{-1} in the simulation gives a good agreement with the experimentation for the frequency of optimal sensitivity.

Nevertheless, it can be noted that the EC signal relative variation is higher in the modelling than in the measurement. Several parameters can explain this difference. Among them are the real geometry of the EC probe that is not modelled precisely and the uncertainties on the values of the SMM parameters and of the lift-off. Tests are underway in order to validate these hypotheses.

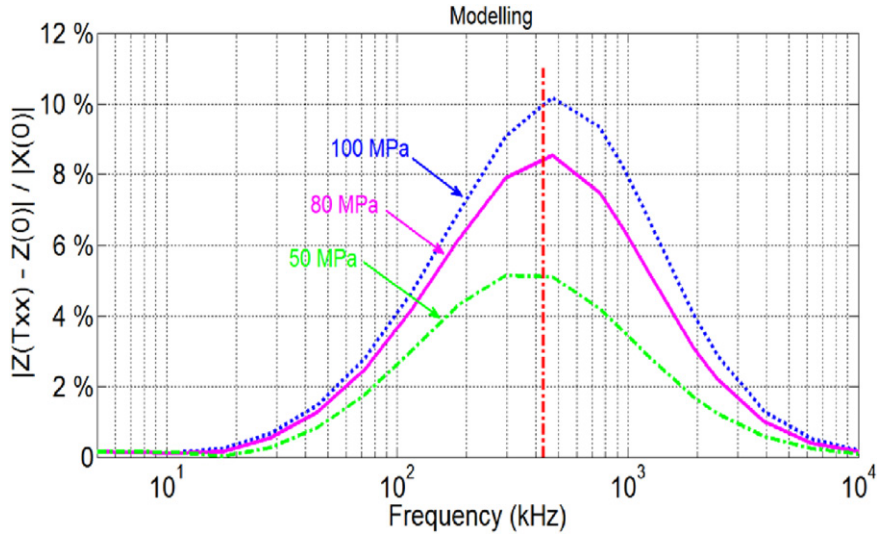


Figure 10. Simulated variations of impedance Z for different levels of tensile stress (50, 80 and 100 MPa) as a function of frequency. The results are normalised by the reactance $X(0)$ in the unstressed configuration. The material conductivity is taken as 7 MS m^{-1} .

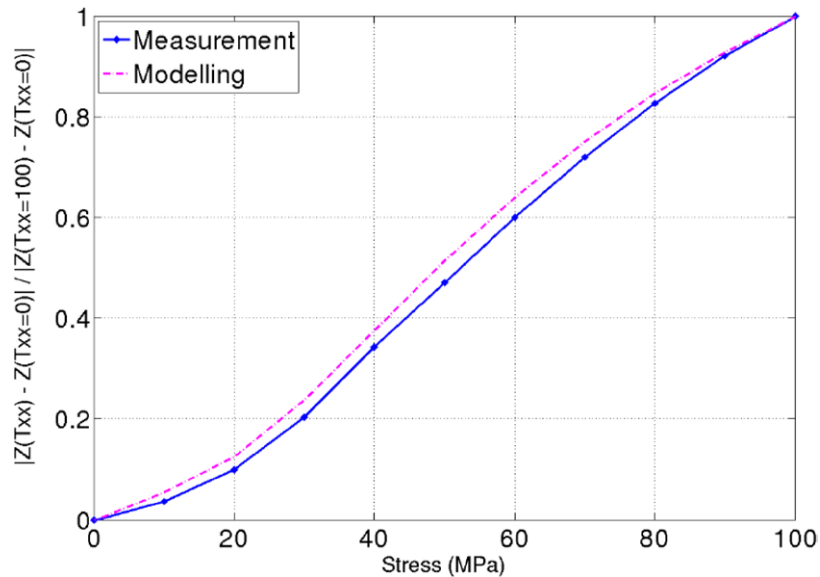


Figure 11. Calibrated variations of the impedance Z as a function of the applied tensile stress: Measurement (plain line) and modelling (dashed line).

Since modelling and experimental results show very similar trends for the impedance as a function of frequency, the quantitative discrepancies in magnitude can be overcome using a calibration procedure. The calibration procedure consists in normalising the impedance variation due to the stress by its value for the maximum considered stress level, rather than as previously by the reactance under no applied stress. Here, the tensile stress ranges from 0 to 100 MPa. The calibrated variation of impedance is then defined by $|Z(T_{xx}) - Z(0)| / |Z(T_{xx} = 100) - Z(0)|$. Figure 11 shows the evolution of this calibrated variation as function of the stress for both experimental and modelling results. The results have been extracted at the peak frequency for optimal sensitivity (400 kHz for measurements and 430 kHz for simulation) and for a conductivity of 7 MS m^{-1} in the modelling.

A very good accordance between modelling and experimental results is shown after calibration of the EC measurements. The calibration allows deducing the experimental level of tensile stress from the modelling curve with an error of less than 3 MPa. This result was consolidated by realizing reproducibility tests.

These results clearly show the potentiality of the developed modelling to predict the effect of stress on the EC signal. The size of the inspected volume, and hence the method resolution for the estimation of stress, depends on the size of the EC probe (surface resolution) and on the material properties (depth resolution). The proposed modelling approach can help to design an inspection setup and procedure for a given application.

Several practical issues remain. A magnetic demagnetisation was realised prior to the EC measurements. Performing

the measurement on a magnetised material was found to have an impact on the variations of impedance. The very good precision obtained on demagnetised specimen was then damaged. This effect is attributed to the non-linearity of the magnetic behaviour that influences the value of the magnetic permeability depending on the initial magnetisation state. However, in a practical detection context, a local reference magnetisation state could be obtained by using an auxiliary low-frequency device [12]. Indeed the measurement area is very limited and the reference magnetisation state is only needed locally.

A normalisation procedure was needed to obtain the high precision on the stress evaluation. This is a limitation of the method since a measurement is then needed on a reference specimen. It can be noticed however that in an industrial context, this normalisation procedure can be performed on a reference area on the sample to be inspected instead of a separate reference sample. Indeed, the critical region of an industrial part seldom covers all the part, and selected non critical regions can be used to calibrate the measurement. Such a procedure allows avoiding the effect of the variations in material properties from one fabrication lot to another notably in relation to the fabrication process.

8. Conclusion

EC NDE is a promising technique to evaluate stress in magnetic materials. This paper proposes a methodology for the modelling of stress detection using the EC technique. In absence of any calibration with the material under stress, first results show a good qualitative accordance between the modelling (figure 10) and the measurement (figure 7) and therefore validate the principle of the modelling approach. A good quantitative agreement between modelling and measurements (figure 11) necessitates a calibration procedure to deal with the sensitivity to material properties or probe geometry. For the Iron–Cobalt alloy tested in this study, it is shown that a uniaxial tensile stress can be detected with an error lower than 3 MPa in the range from 0 to 100 MPa using the proposed modelling tool. In an industrial context the calibration can be performed either on a separate reference sample or on a reference region of the sample to be inspected.

The developed model can be used to study and select the most efficient EC probes and to define optimal operating conditions, including notably the frequency of the measurement. Moreover, in the context of stress evaluation where an inversion procedure is required, the use of a physical-based constitutive magneto-elastic model will typically require less identification and calibration procedures than a brute fitting of experimental data (e.g. polynomial fitting or neural networks).

Although the proposed numerical tool allows taking into account multiaxial stresses configurations, the method was only applied in a pure tension configuration. As long as the constitutive equations remain valid, the multiaxiality of stress is not a real problem for the direct simulation. It becomes a challenge when the stress state is to be deduced from the measurements. Indeed different stress state could affect the material permeability similarly. This problem could be

handled with advanced inversion tools taking better advantage of the anisotropy induced by the application of stress. For that purpose, several measurements with different orientations for the U-core could be combined together. The coupling between stress and frequency effects [35] could also be exploited by analysing the results at different frequencies. A prior knowledge of the form of the stress tensor, as it is often the case in practical NDE, could of course be used as a significant simplification of the inverse problem.

Acknowledgments

The authors thank Prof O Hubert at LMT-Cachan for his help in providing the ferromagnetic samples.

References

- [1] Withers P J and Bhadeshia H K D H 2001 Residual stress part I—measurement techniques *Mater. Sci. Technol.* **17** 355–65
- [2] Cohen J B and Noyan I C 1987 *Residual Stress—Measurement by Diffraction and Interpretation* (New York: Springer)
- [3] Almer J D and Winholtz R A 2008 *X-ray Stress Analysis in Handbook of Experimental Solid Mechanics* ed W N Sharpe (New York: Springer)
- [4] Jiles D C 1988 Review of magnetic methods for nondestructive evaluation *NDT Int.* **21** 311–9
- [5] Jiles D C 1990 Review of magnetic methods for nondestructive evaluation part 2 *NDT Int.* **23** 83–92
- [6] Bozorth R M 1951 *Ferromagnetism* (New York: Van Nostrand)
- [7] Cullity B D and Graham C D 2011 *Introduction to Magnetic Materials* (New York: Wiley)
- [8] Langman R A and Mutton P J 1993 Estimation of residual stresses in railway wheels by means of stress-induced magnetic anisotropy *NDT&E Int.* **26** 195–205
- [9] Buttle D and Scruby C 2001 Residual stress: measurement using magnetoelastic effects *The Encyclopaedia of Materials: Science and Technology* (Oxford: Pergamon)
- [10] Lo K H, Buttle D and Mummery P 2002 The effects of service lifetime and duty on the residual stresses in railway rails *Mater. Sci. Forum* **404–7** 761–6
- [11] Altpeter I, Becker R, Dobmann G, Kern R, Theiner W and Yashan A 2002 Robust solutions of inverse problems in electromagnetic non-destructive evaluation *Inverse Problems* **18** 1907–21
- [12] Dobmann G, Altpeter I, Wolter B and Kern R 2008 Industrial applications of 3MA—micromagnetic multiparameter microstructure and stress analysis *Stud. Appl. Electromagn. Mech.* **31** 18–25
- [13] Wilson J W, Tian G Y and Barrans S 2007 Residual magnetic field sensing for stress measurement *Sensors Actuators A* **135** 381–7
- [14] Roskosz M and Bieniek M 2012 Evaluation of residual stress in ferromagnetic steels based on residual magnetic field measurements *NDT&E Int.* **45** 55–62
- [15] Roskosz M and Bieniek M 2013 Analysis of the universality of the residual stress evaluation method based on residual magnetic field measurements *NDT&E Int.* **54** 63–8
- [16] Abuku S and Cullity B D 1971 A magnetic method for the determination of residual stress *Exp. Mech.* **11** 217–23
- [17] Chady T, Sikora R, Psuj G, Enokizono M and Todaka T 2005 Fusion of electromagnetic inspection methods for evaluation of stress-loaded steel samples *IEEE Trans. Magn.* **41** 3721–3

- [18] Schoenekeess H C, Ricken W and Becker W J 2007 Method to determine tensile stress alterations in prestressing steel stands by means of an eddy-current technique *IEEE Sensors J.* **7** 1200–5
- [19] Daniel L, Hubert O, Buiron N and Billardon R 2008 Reversible magneto-elastic behavior: a multiscale approach *J. Mech. Phys. Solids* **56** 1018–42
- [20] Daniel L and Galopin N 2008 A constitutive law for magnetostrictive materials and its application to terfenol-D single and polycrystals *Eur. Phys. J. Appl. Phys.* **42** 153–9
- [21] Blodgett M P and Nagy P B 2004 Eddy current assessment of near-surface residual stress in shot-peened nickel-base superalloys *J. Nondestruct. Eval.* **23** 107–23
- [22] Morozov M, Tian G Y and Withers P J 2010 The pulsed eddy current response to applied loading of various aluminium alloys *NDT&E Int.* **43** 493–500
- [23] Rao B P C 2007 *Practical Eddy Current Testing* (Oxford: Alpha Science)
- [24] Le Bihan Y 2003 Study on the transformer equivalent circuit of eddy current nondestructive evaluation *NDT&E Int.* **36** 297–302
- [25] Galopin N, Daniel L, Bouillault F and Besbes M 2007 Numerical analysis for the design of a magneto-elastic characterisation device *El. Rev./Prz. Elektrotech.* **83** 44–7
- [26] Bernard L, Mininger X, Daniel L, Krebs G, Bouillault F and Gabsi M 2011 Effect of stress on switched reluctance motors: a magneto-elastic finite-element approach based on multiscale constitutive laws *IEEE Trans. Magn.* **47** 2171–8
- [27] Armstrong W D 2002 A directional magnetization potential based model of magnetoelastic hysteresis *J. Appl. Phys.* **91** 2202
- [28] Buiron N, Hirsinger L and Billardon R 1999 A multiscale model for magneto-elastic couplings *J. Phys. IV* **9** 187
- [29] Daniel L, Rekik M and Hubert O 2014 A multiscale model for magneto-elastic behaviour including hysteresis effects *Arch. Appl. Mech.* **84** 1307–23
- [30] Chang H, Schoenig F C and Soules J A 1999 Eddy current offers a powerful tool for investigating residual stress and other metallurgical properties *Mater. Eval.* **57** 1257–60
- [31] Bastos J P A and Sadowski N 2003 *Electromagnetic Modelling by Finite Element Methods* vol 1 (New York: Marcel Dekker)
- [32] Ren Z and Razek A 1996 Computation of 3D electromagnetic field using differential forms based elements and dual formulation *Int. J. Numer. Modelling: Electron. Netw. Devices Fields* **9** 81–98
- [33] www.magmet.com/nam/images/NAM_cat_combinedCh5.pdf
- [34] Bertotti G, Fiorillo F and Soadro G P 1988 The prediction of power losses in soft magnetic materials *J. Phys.* **49** 1915–8
- [35] Rekik M, Hubert O and Daniel L 2014 Influence of a multiaxial stress on the reversible and irreversible magnetic behaviour of a 3% Si-Fe alloy *Int. J. Appl. Electromagn. Mech.* **44** 301–15